ARTICLE

PyrroTriPol: a Semi-rigid Trityl-Nitroxide for High Field Dynamic Nuclear Polarization

Thomas Halbritter,[†a] Rania Harrabi,[†b] Subhradip Paul,[b] Johan van Tol,[c] Daniel Lee,[b#] Sabine Hediger,[b] Snorri Th. Sigurdsson,*[a] Frédéric Mentink-Vigier,*[c] Gaël De Paëpe *[b]

Table of Contents

[a.] *University of Iceland, Department of Chemistry, Science Institute, Dunhaga 3, 107 Reykjavik, Iceland.*
[b.] *Univ. Grenoble Alpes, CEA, CNRS, IRIG, MEM, 38000 Grenoble, France.*
[c.] *National High Magnetic Field Laboratory, Florida State University, Tallahassee, FL, 32301, USA.*
[#.] *Department of Chemical Engineering, University of Manchester; Manchester, M13 9PL, UK*
Emails: snorrisi@hi.is,, fmentink@magnet.fsu.edu, gael.depaepe@cea.fr
† These authors contributed equally

Abbreviations

aq.	aqueous
BOP	(benzotriazol-1-yloxy)-tris-(dimethylamino)-phosphonium-hexafluorophosphat
CH_2Cl_2	dichloromethane
CP	cross polarization
DCC	dicyclohexyl carbodiimide
DCE	dichloroethane
DMF	*N*,*N*-dimethylformamide
DNP	dynamic nuclear polarization
DIPEA	*N*,*N*-diisopropylethylamine
ESI-HRMS	electron spray ionization high resolution mass spectrometry
EPR	electron paramagnetic resonance
EtOAc	ethyl acetate
Et_3N	triethylamine
hBN	hexagonal boron nitride
HOBt	1-hydroxybenzotriazol
HPLC	high performance liquid chromatography
MAS	magic angle spinning
NMR	nuclear magnetic resonance
Pet. ether	petroleum ether
Satd.	saturated
T_B	buildup time
TCE	1,1,2,2-tetrachloroethane
TFA	trifluoroacetic acid
TLC	thin layer chromatography
UV	ultra violet

General materials and methods

All commercially available reagents were purchased from Sigma-Aldrich, Inc. or Acros Organics and used without further purification. All moisture- and air-sensitive reactions were carried out in oven-dried glassware under an inert atmosphere of Ar. Thin-layer chromatography (TLC) was performed using glass plates pre-coated with silica gel (0.25 mm, F-25, Silicycle) and compounds were visualized under UV light. Column chromatography was performed using 230–400 mesh silica gel (Silicycle). Radicals show broadening and loss of NMR signals due to their paramagnetic nature and, therefore, those NMR spectra are not shown. EPR spectra were recorded on a MiniScope MS200 (Magnettech Germany) spectrometer. Mass spectrometric analyses of all organic compounds were performed on an ESI-HRMS (Bruker, MicrOTOF-Q) in a positive ion mode.

Purification of **TEMTriPol-I**, **DiTEMTriPol-I**, **PyrroTriPol and DiPyrroTriPol** was performed on a preparative Agilent HPLC system using a GL Sciences Inertsustain C18 14×250 mm column with UV detection at λ = 254 nm with a flow rate of 10 mL/min using the following gradient: Solvent A, H_2O; solvent B, CH_3CN; 0-4 min isocratic 4% B, 4-20 min gradient 4-100% B, 20-21 min isocratic 100% B, 21-23 min 100-4% B.

Purity of all biradicals was analysed on an analytical Agilent HPLC system using a Pursuit 5 C18 4.6x250 mm analytical column with UV detection at λ = 254 nm with a flow rate of 1 mL/min using an isocratic run for **TEMTriPol-I-OMe**, **DiTEMTriPol-I-OMe**, **PyrroTriPol-OMe** and **DiPyrroTriPol**: 0-16 min 100% CH_3CN 16 min, and for **TEMTriPol-I** and **PyrroTriPol** the following gradient: Solvent A, 0.1% TFA in MilliQ-H_2O; solvent B, CH_3CN; 0-4 min isocratic 4% B, 4-30 min gradient 4-100% B, 30-34 min isocratic 100% B, 34-35 min 100-4% B.

Synthetic protocols

PyrroTriPol and PyrroTriPol-OMe

General scheme for synthesis of trityl monoradical as precursor

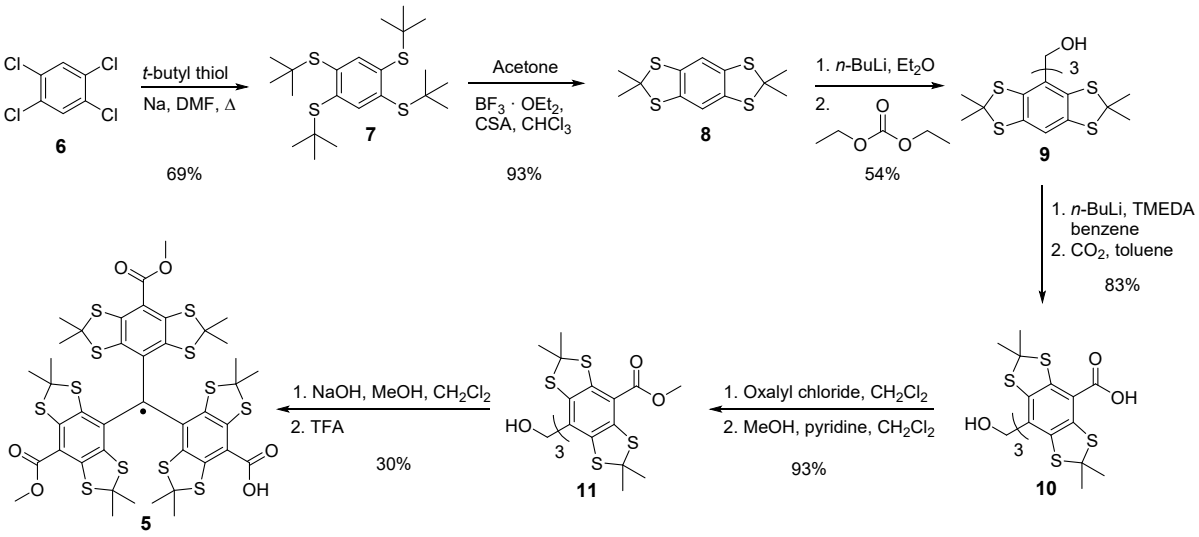

Scheme 1. Synthesis of trityl mono radical.

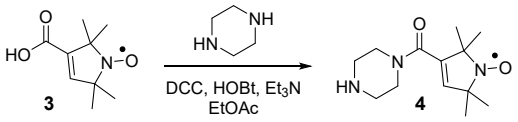

Piperazine nitroxide 4. To a solution of nitroxide **3** (0.100 g, 0.54 mmol) in EtOAc (5.0 mL) was added DCC (0.167 g, 0.81 mmol) and HOBt (0.124 g, 0.81 mmol) and the resulting solution was stirred at 22 °C for 5 min and added dropwise to a solution of piperazine (0.140 g, 1.63 mmol) in EtOAc (10 mL) and Et_3N (0.11 mL, 0.81 mmol). The reaction mixture was stirred at 22 °C for 12 h. The precipitate was filtered off, the solvent was removed *in vacuo* and the residue purified by column chromatography (CH_2Cl_2:MeOH, 9:1 + 0.1% Et_3N) to yield piperazine nitroxide **4** (0.108 g, 79%) as yellow solid.

TLC (Silica gel, CH_2Cl_2:MeOH 9:1), Rf (**piperazine nitroxide 4**) = 0.1

ESI-HRMS: calcd. for $C_{13}H_{22}N_3O_2$ [M+H$^+$] 253.1785, measured 253.1776 (Δm = 0.0009, error = 3.6 ppm).

EPR (DCE, 1.0 mM):

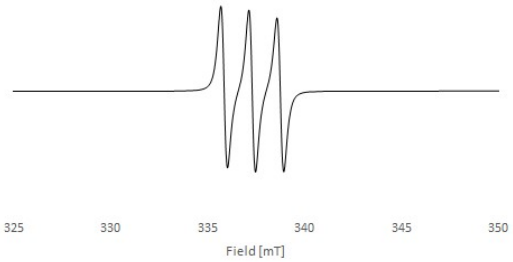

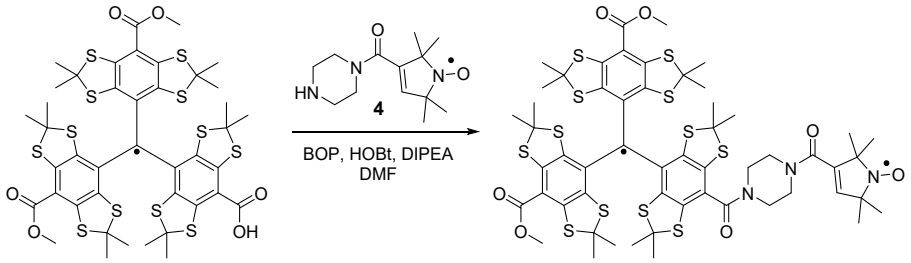

5 **PyrroTriPol-OMe**

PyrroTriPol-OMe. To a solution of trityl **5** (0.030 g, 0.029 mmol) in DMF (2.0 mL) was added BOP (0.020 g, 0.044 mmol), HOBt (0.006 g, 0.044 mmol) and DIPEA (0.008 mL, 0.044 mmol) and the resulting solution was stirred at 22 °C for 5 min. Nitroxide **4** (0.008 g, 0.032 mmol) was added to the solution and the resulting reaction mixture was stirred at 22 °C for 12 h. Satd. aq. $NaHCO_3$ (10 mL) was added and the solution extracted with EtOAc (3x10 mL). The combined organic layers were dried over Na_2SO_4, the solvent was removed *in vacuo* and the residue purified by flash column chromatography (pet. ether: EtOAc, 6:4) to give **PyrroTriPol-OMe** (0.033 g, 88% yield) as a green solid.

TLC (Silica gel, pet. ether:EtOAc 1:1), Rf (**PyrroTriPol-OMe**) = 0.4

ESI-HRMS: calcd. for $C_{55}H_{63}N_3O_7S_{12}$ [M+Na^+] 1284.1207, measured 1284.1164 (Δm = 0.0043, error = 3.3 ppm).

EPR (DCE, 1.0 mM):

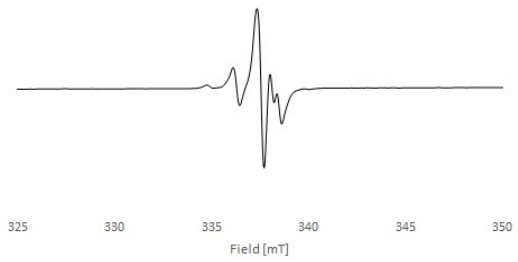

HPLC

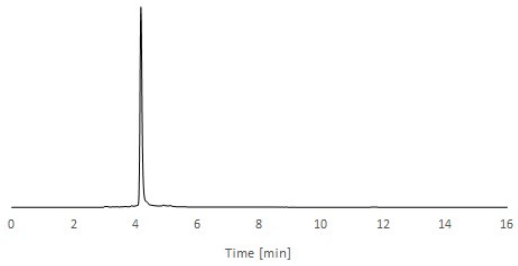

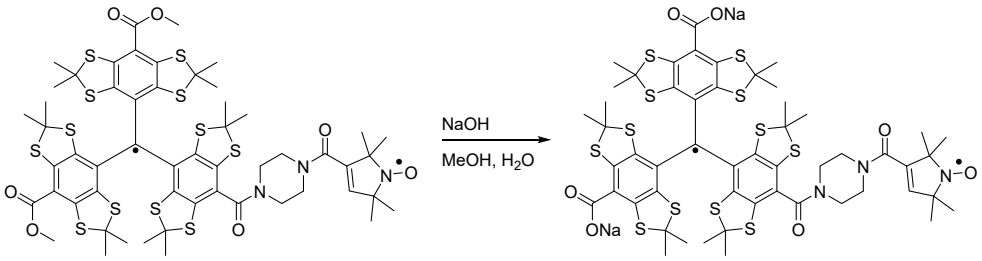

PyrroTriPol-OMe **PyrroTriPol**

PyrroTriPol. To a solution of **PyrroTriPol-OMe** (0.015 g, 0.012 mmol) in MeOH (2.0 mL) was added NaOH (0.003 g, 0.072 mmol) and H_2O (0.1 mL). The reaction mixture was stirred at 22 °C for 48 h. The solvent was removed *in vacuo* and the residue purified by C18-HPLC to afford **PyrroTriPol** (0.013 g, 86% yield) as a green solid.

ESI-HRMS: calcd. for $C_{53}H_{59}N_3O_7S_{12}$ [M-H^+] 1232.0929, measured 1232.0922 (Δm = 0.0007, error = 0.6 ppm).

EPR (H_2O, 1.0 mM):

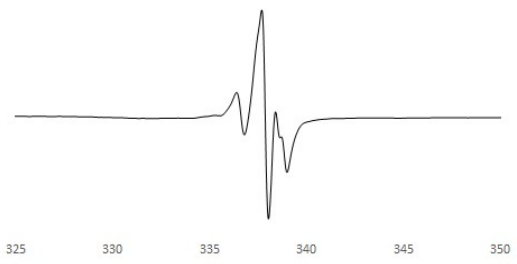

HPLC

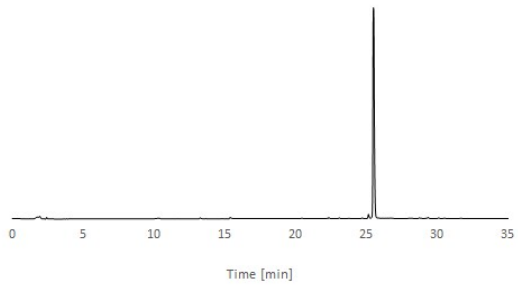

TEMTriPol-I and TEMTriPol-I-OMe

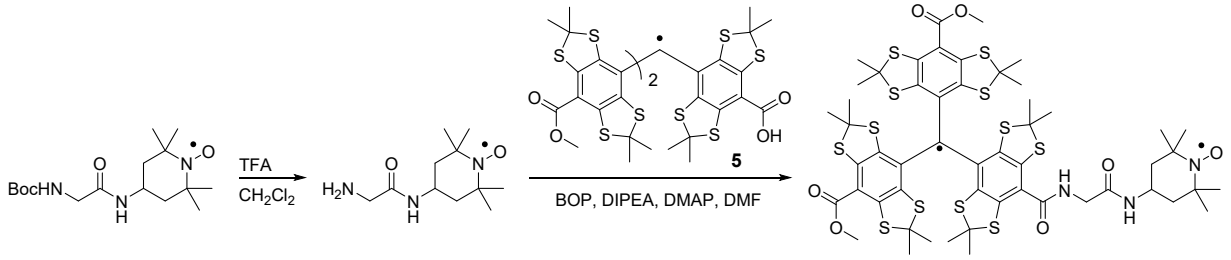

TEMTriPol-I-OMe. To a solution of BOC-Gly-Tempo (**1**) (0.015 g, 0.044 mmol, 2.0 eq) in CH_2Cl_2 (1 mL) was added TFA (1 mL) dropwise at 0 °C and the resulting solution was stirred at 22 °C for 3 h. The solvent was removed *in vacuo* to give amino-Gly-Tempo (**2**) which was used without further purification.
To a solution of trityl **5**[1,2] (0.030 g, 0.029 mmol) in DMF (2.0 mL) was added BOP (0.020 g, 0.044 mmol), HOBt (0.006 g, 0.044 mmol) and DIPEA (0.012 mL, 0.066 mmol) and the resulting solution stirred at 22 °C for 5 min. Nitroxide **2** (0.010 g, 0.044 mmol) was added to the solution and the resulting reaction mixture was stirred at 22 °C for 12 h. Satd. aq. $NaHCO_3$ (10 mL) was added and the solution extracted with EtOAc (3x10 mL). The combined organic layers were dried over Na_2SO_4, the solvent was removed *in vacuo* and the residue purified by flash column chromatography (pet. ether: EtOAc, 6:4) to give **TEMTriPol-I-OMe** (0.022 g, 63% yield) as green solid.

TLC (Silica gel, pet. ether:EtOAc 1:1), Rf (**TEMTriPol-I-OMe**) = 0.3

ESI-HRMS: calcd. for $C_{53}H_{63}N_3O_7S_{12}$ [M+Na$^+$] 1260.1207, measured 1260.1198 (Δm = 0.0009, error = 0.7 ppm).

EPR (DCE, 1.0 mM):

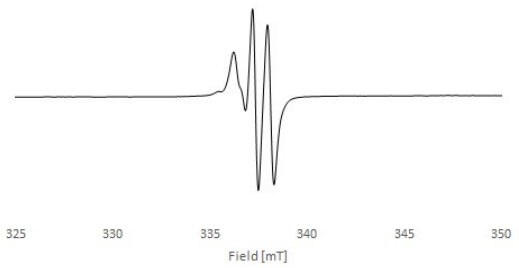

HPLC

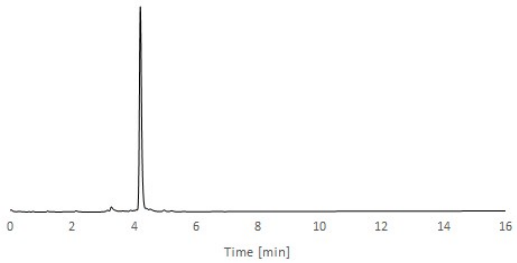

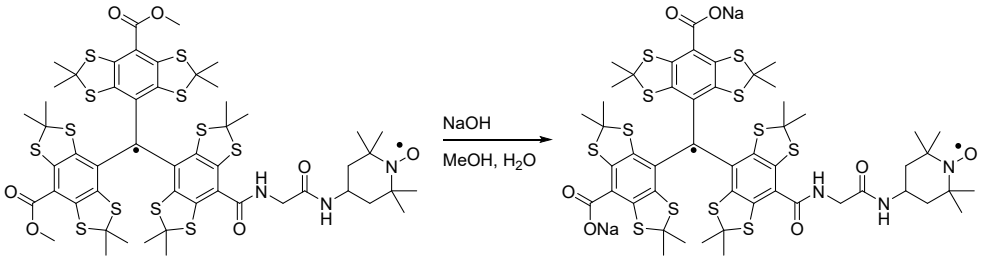

TEMTriPol-I-OMe **TEMTriPol-I**

TEMTriPol-I. To a solution of **TEMTriPol-I-OMe** (0.015 g, 0.012 mmol) in MeOH (2.0 mL) was added NaOH (0.003 g, 0.072 mmol) and H_2O (0.1 mL). The reaction mixture was stirred at 22 °C for 48 h. The solvent was removed *in vacuo* and the residue purified by C18-HPLC to give **TEMTriPol-I** (0.004 g, 28% yield) as a green solid.

ESI-HRMS: calcd. for $C_{51}H_{58}N_3O_7S_{12}$ [M-H$^+$] 1208.0929, measured 1208.0875 (Δm = 0.0054, error = 4.5 ppm).

EPR (H_2O, 1.0 mM):

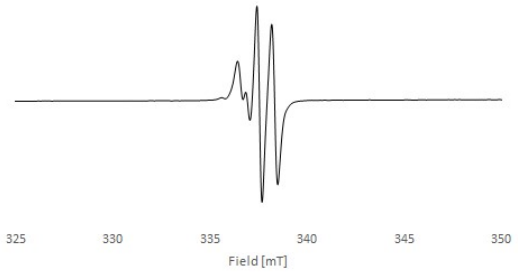

HPLC

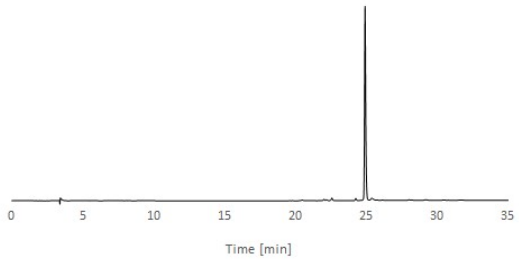

DiPyrroTriPol-OMe

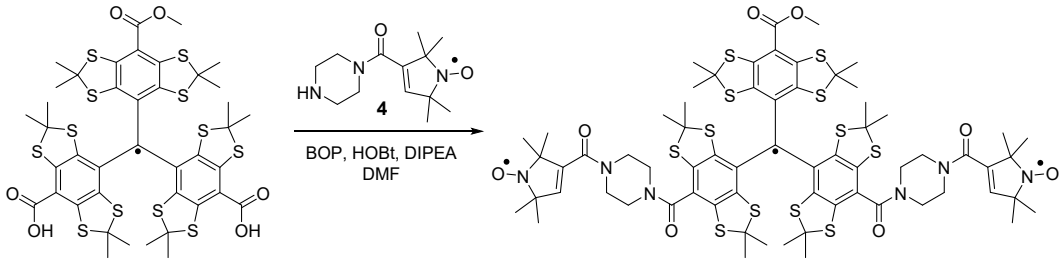

12 **DiPyrroTriPol-OMe**

DiPyrroTriPol-OMe. To a solution of trityl **12** (0.010 g, 0.010 mmol) in DMF (1.0 mL) was added BOP (0.013 g, 0.030 mmol), HOBt (0.004 g, 0.030 mmol) and DIPEA (0.011 mL, 0.060 mmol) and the resulting solution was stirred at 22 °C for 5 min. Nitroxide **4** (0.008 g, 0.030 mmol) was added and the resulting solution was stirred at 22 °C for 12 h. Satd. $NaHCO_3$ (10 mL) was added and the solution extracted with EtOAc (3x10 mL). The combined organic layers were dried over Na_2SO_4, the solvent was removed *in vacuo* and the residue purified by flash column chromatography (pet. ether: EtOAc, 3:7) to give **DiPyrroTriPol-OMe** (0.013 g,0.009 mmol, 88% yield) as a green solid.

TLC (Silica gel, pet. ether:EtOAc 3:7), Rf (**DiPyrroTriPol-OMe**) = 0.4

ESI-HRMS: calcd. for $C_{67}H_{81}N_6O_8S_{12}$ [M+Na$^+$] 1504.2657, measured 1504.2583 (Δm = 0.0074, error = 4.9 ppm).

EPR ($ClCH_2CH_2Cl$, 1.0 mM):

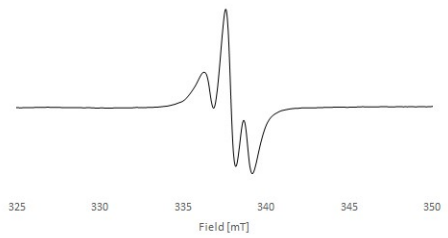

HPLC

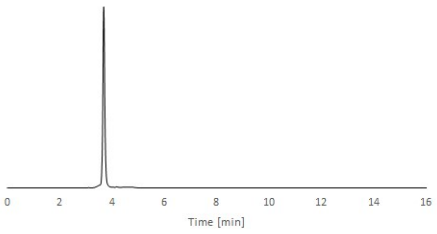

DiTEMTriPol-I-OMe

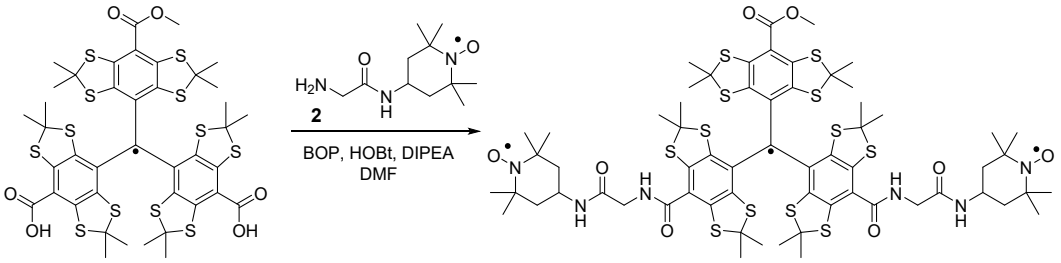

12 **DiTEMTriPol-I-OMe**

DiTEMTriPol-I-OMe. To a solution of trityl **12** (0.010 g, 0.010 mmol) in DMF (1.0 mL) was added BOP (0.013 g, 0.030 mmol), HOBt (0.004 g, 0.030 mmol) and DIPEA (0.011 mL, 0.060 mmol) and the resulting solution was stirred at 22 °C for 5 min. Nitroxide **2** (0.007 g, 0.030 mmol) was added and the resulting reaction solution was stirred at 22 °C for 12 h. Satd. $NaHCO_3$ (10 mL) was added and the solution extracted with EtOAc (3x10 mL). The combined organic layers were dried over Na_2SO_4, the solvent was removed *in vacuo* and the residue purified by flash column chromatography (pet. ether: EtOAc, 3:7) to give **DiTEMTriPol-I-OMe** (0.008 g,0.005 mmol, 54% yield) as a green solid.

TLC (Silica gel, pet. ether:EtOAc 3:7), Rf (**DiTEMTriPol-I-OMe**) = 0.3

ESI-HRMS: calcd. for $C_{63}H_{81}N_6O_8S_{12}$ [M+Na^+] 1456.2657, measured 1456.2625 (Δm = 0.0032, error = 2.2 ppm).

EPR ($ClCH_2CH_2Cl$, 1.0 mM):	HPLC
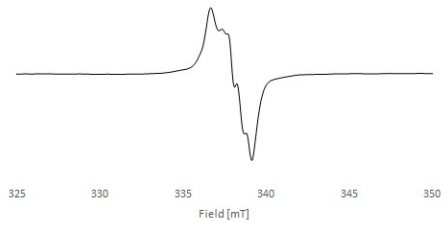	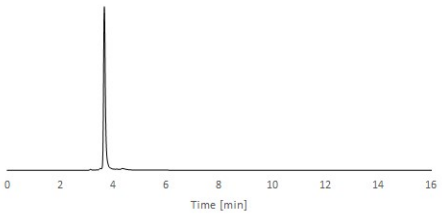

DFT and MD simulations for EPR fitting

MD, main conformers of TEMTriPol-I and PyrroTriPol

The structures were first optimized with DFT using ORCA v5.0 [3] and PBEh-3c[4] as optimization method. The charges were obtained from the optimized structure using B3LYP[5] and 6-31G(d,p), followed by a two stage RESP fitting using Multiwfn[6]. From the MD simulations, run using OpenMM[7] in explicit water/glycerol, two major conformers can be extracted for both TEMTriPol-I and PyrroTriPol. The structures have then be re-optimized using r2SCAN-3c[8] and are shown in **Fig S. 1**. The MD simulations predict that conformer (b) is the main one for TEMTriPol-I, conformer (c) is the main one for PyrroTriPol.

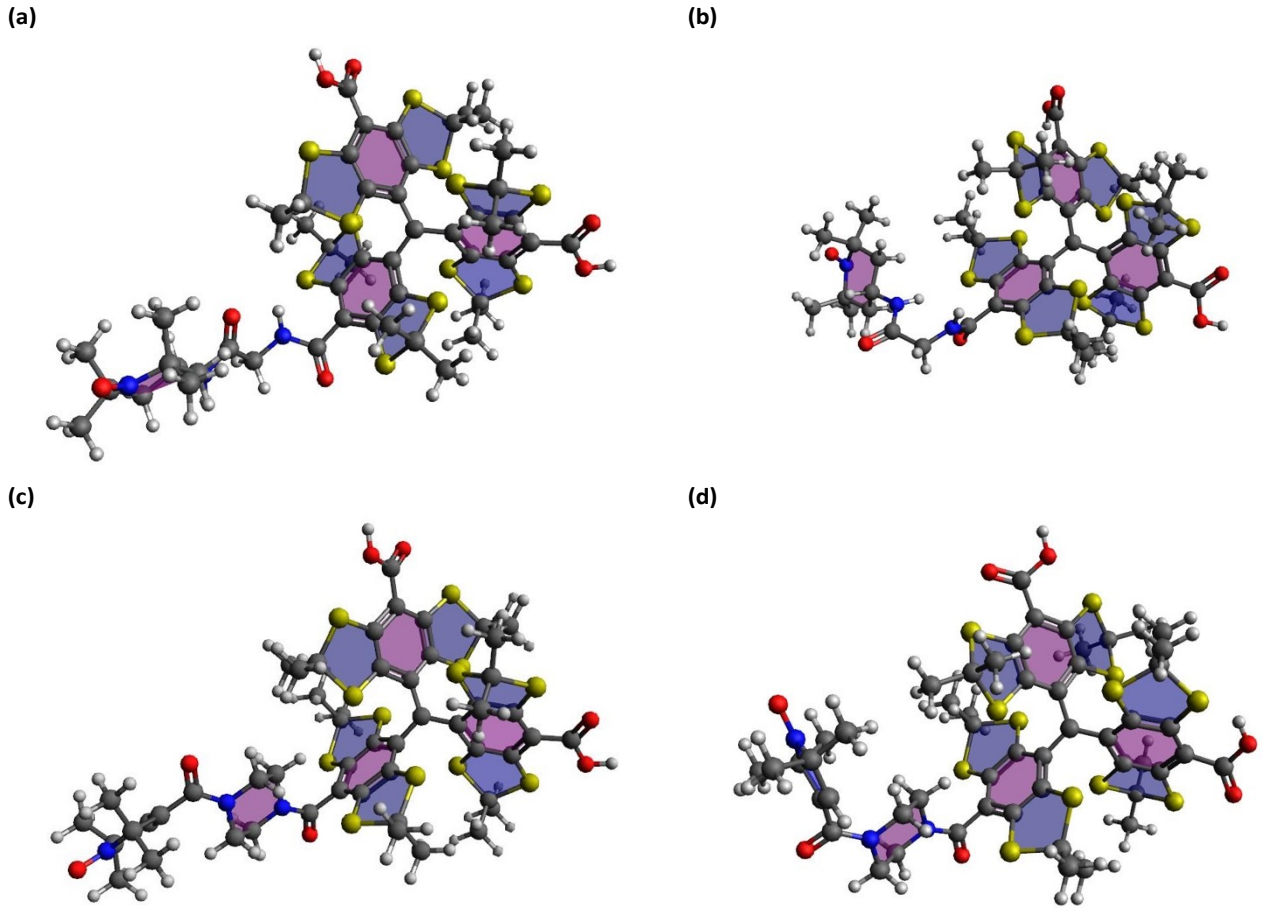

Fig S. 1 (a) and (b) major conformers of TEMTriPol-I; (c) and (d) major conformers of PyrroTriPol

DFT and EPR fits with main conformers of TEMTriPol-I and PyrroTriPol

From these structures it is possible to extract the g-tensors, and the dipolar and exchange couplings of the biradicals. The g-tensors were obtained using PBE0[9] and def2-TZVP[10] basis, the exchange interaction was obtained with tight convergence of CAM-B3LYP[5] using def2-SVP[10] basis. The predicted values, used for reproducing the spectra are reported in Table S1. We used the same notations as previously.[11,12]

Table S1 Predicted and fitted (in bold) magnetic properties for the major conformers of TEMTriPol-I and PyrroTriPol

Biradical	[gxx, gyy, gzz] Tempo [gxx, gyy, gzz] Trityl **Bold correspond to fitted values**	Relative orientation [α,β,γ] (degrees)	Dipolar ($D_{a,b}$)/exchange ($J_{a,b}$) **(bold correspond to the fitted value)** (MHz)	Dipolar vector [ϕ,θ] (degrees)	^{14}N hyperfine coupling (MHz)	% Exp. Contribution
TEMTriPol-I extended (S2,a)	[2.0091 **(2.0088)**,2.0061,2.0021] [2.0024,2.0029,2.0036]	[175 35 99]	25 / -17 **(-8.5)**	[25, 92]	[18,18,102]	50%
TEMTriPol-I contracted (S2,b)	[2.0091 **(2.0088)**,2.0062,2.0021] [2.0024,2.0029,2.0036]	[115 53 140]	42 / -25	[24 ,53]	[18,18,102]	50%
PyrroTriPol extended (S2,c)	[2.0088 **(2.0082)**,2.0059,2.0021] [2.0024,2.0029,2.0036]	[163, 92, 26]	21 / -4 **(-8)**	[-16, 101]	[14,14,100]	80%
PyrroTriPol contracted (S2,d)	[2.0088 **(2.0082)**,2.0059,2.0021] [2.0024,2.0029,2.0036]	[115, 130, 20]	43 / -30 **(-35)**	[17 27]	[14,14,100]	20%

The EPR spectra of TEMTriPol-I and PyrroTriPol (**Fig S. 2**) were recorded at 240 GHz as previously described[11,12] on a custom built multi-frequency instrument[13]. The spectrum of TEMTriPol-I is reminiscent of previously reported spectra.[14,15] It presents a shoulder next to the trityl region, which can be attributed to a conformer with large e-e couplings.[14,15] On the contrary, PyrroTriPol does not show such broadening or a shoulder, and the trityl line remains "narrow". However, we observe the presence of a signal close to 8.565 T, marked with a star in **Fig S. 2**. This signal is smaller in the EPR spectrum of PyrroTriPol at 5 vs 10 mM, shown in **Fig S. 4**. As this signal diminishes for lower biradical concentration, we attributed it to the formation of aggregates.

The experimental EPR spectra at 240 GHz were partially fitted by adjusting the g_{xx} value of the nitroxide, the exchange interaction and the relative ratio of the two conformers using Easyspin.[16] The corresponding fits are reported in **Fig S. 2**. The Easyspin "pepper" method that aims at computing solid-state EPR spectra, was combined with the Easyspin "hybrid" approach, which applies diagonalization to the electron spin subspace and perturbation to the nuclear subspace. We assumed a line broadening arising from a mixture of Gaussian and Lorentzian lineshape of width [0.4 0.4] mT respectively. The fit of the adjustment of the g values led to g_{xx} = 2.0088 for TEMTriPol-I and gxx = 2.0082 for PyrroTriPol.

For PyrroTriPol, 80% of the spectrum is made of the extended conformer, 20% of the contracted conformer and the exchange interaction are slightly lower than predicted. This ratio 8/2 ratio is in good agreement with the MD simulations for PyrroTriPol that predict a bimodal distribution, centred on 13.8 and 11.5 angstroms, with a ratio close to 8/2.

For TEMTriPol-I, the extended and contracted conformers have the same proportion. There was no need to adjust the exchange value of the contracted conformer while the DFT simulation seems to have slightly overestimated it by a factor 2. The agreement between the EPR data and the fitted spectrum is reasonable despite the existence of a distribution conformation. This comment extends to previously recorded EPR data at 285 GHz.

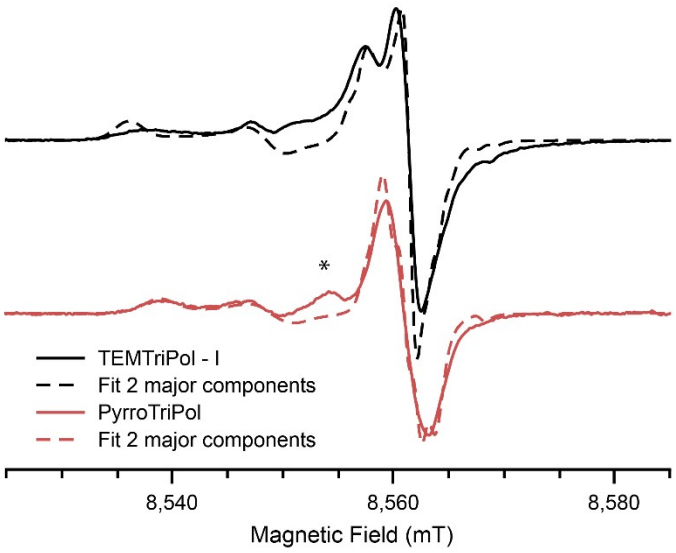

Fig S. 2 EPR spectra at 240 GHz of TEMTriPol-I at 10 mM (black) and PyrroTriPol at 5 mM (red) measured at 100 K. The fitted EPR spectra are reported as dashed line. The *signal marked with an asterisk is attributed to aggregation.

The fitted parameters of TEMTriPol-I were used to predict the EPR spectrum at 285 GHz and compare it to previously published data[15]. The spectra are shown in **Fig S. 3**. The agreement between experiment and simulation is surprisingly correct. Indeed MD simulations indicate a significant flexibility, and the current fit only accounts for two conformations.

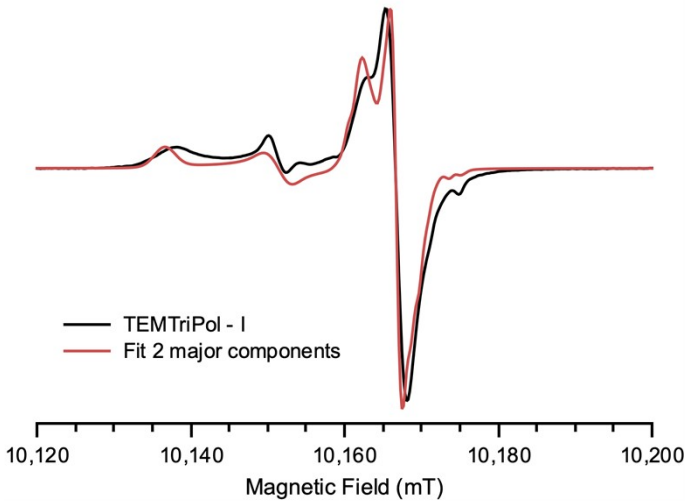

Fig S. 3 EPR spectra at 285 GHz of TEMTriPol-I at 10 mM (black) and the predicted EPR spectra based on the 240 GHz fit

Effect of concentration on the EPR spectrum of PyrroTriPol

Fig S. 4 reports the EPR spectrum of PyrroTriPol in the DNP matrix collected at 240 GHz at 100 K for two concentrations, 5 and 10 mM. We observe a change in the EPR spectra, close to 8.565 T. An additional signal is present and much stronger at 10 mM than 5 mM. This signal may be the sign of partial aggregation of the biradical, more preeminent at 10 mM than 5 mM.

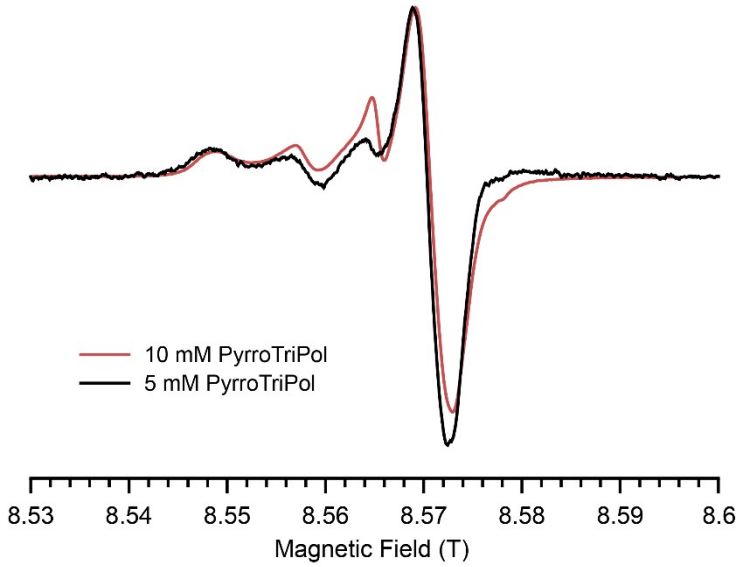

Fig S. 4 EPR spectra at 240 GHz of PyrroTriPol at 5 mM (black) and 10 mM (red) measured at 100 K

Data analysis and DNP evaluation

The evaluation of the enhancement factor $\varepsilon_{On/Off}$ was based on the intensity ratio of the ^{13}C CP-MAS spectra recorded with (S_{On}) and without (S_{Off}) μwave irradiation:

$$\varepsilon_{On/Off} = \frac{S_{On}}{S_{Off}}$$

To evaluate the depolarization factor $\varepsilon_{depo,}$ we relied on the recorded ^{1}H spectrum and used the procedure proposed by Q. Chen *et al.* [17] to minimize the proton background signal. The procedures require the acquisition of both a $\pi/2$-pulse and a π-pulse ^{1}H spectrum in absence of μwaves, which are combined to obtain a ^{1}H sample signal with highly reduced background intensity. The procedure was repeated at the spinning frequencies of 0 kHz, 2 kHz, 4 kHz and 8 kHz, with a relatively long recycle delay (D_1) of 30 s at 9.4 T and 60-80 s at 14.1 T. ε_{depo} as a function of the MAS frequency was obtained as the intensity ratio of the corrected ^{1}H signal at the corresponded MAS frequency with the one under static condition (at 0 kHz MAS).

$$\epsilon_{Depo} = \frac{S_{\nu\ kHz}}{S_{0\ kHZ}}$$

The DNP sensitivity is given as the integral of the ^{13}C CP-MAS spectrum with μwave on, I_{on} , keeping all experimental parameters identical throughout each series, divided by the square root of the ^{1}H buildup time T_B:

$$DNP\ sensitivity = \frac{I_{on}}{\sqrt{T_B}}$$

The DNP sensitivity was measured at 8 kHz MAS, both at 9.4 and 14.4 T. The ^{1}H buildup time constant (T_B) was measured through saturation-recovery experiments. For the frozen radical solutions, the resulting T_B curves could be fitted using a mono-exponential function. For the impregnated microcrystalline samples (Figure 7, cellulose and adenosine), a two-component buildup function was required to fit the data, and the optimum recycle delay T_{opt} is defined as described in the Supporting Information of ref. [12].
For the specific case of 40 kHz and 18.8T related to Figure 8, due to time restriction we could not carefully check the depolarization factors ε_{Depo} due to the large 1H proton background.[18] We also report the DNP enhancement per square root of time calculated as:
$\frac{\varepsilon_{on/off}}{\sqrt{T_B}}$

Error bars:
The error on the DNP sensitivity is estimated as follows:

$$\Delta DNP\ sensitivity = DNP\ sensitivity \times \left(\frac{\Delta I_{on}}{I_{on}} + \frac{\Delta T_B}{2T_B}\right)$$

The errors on I_{on} , ΔI_{on}, and on T_B, ΔT_B,were obtained by repeating three times the entire sample preparation procedure and the DNP measurements of each sample. The largest error on I_{on} and T_B were found to be ~10% and 10 %, respectively. These values were then applied to all data series, even if it overestimated the error of some of the data points.
The error estimation of $\varepsilon_{On/Off}$ was performed similarly. The largest error was found to be 5% and was applied to all data series.

At 18.8 T and using 1.3 mm rotors, the sensitivity uncertainty is larger due to the challenge of weighting the packed samples and the possibility of bubbles inside the sample. Due to the limited access time, we could not repeat the experiments and are thus attributing a larger $\Delta I_{on} / I_{on} = 20$ % for those experiments.

Experimental procedures for DNP-enhanced ssNMR experiments

General considerations

The experiments were carried out on Bruker Avance III spectrometers, operating at 9.4, 14.1 and 18.8 T, equipped with low temperature 3.2 mm (9.4 and 14.4 T) and 1.3 mm (18.8 T) wide-bore MAS probes, equipped with a 263 GHz (9.4 T), 395 GHz (14.1 T) and 527 GHz (18.8 T) gyrotrons. The sample temperature with *μ*wave irradiation was estimated based on previous KBr ^{79}Br T_1 relaxation time measurements,[19] performed on each of the spectrometer/probe configuration used in this work. These values correspond to 106 K at 9.4 T on a 1.3 mm probe with MAS = 40 kHz, 105 K at 9.4 Ton a 3.2 mm probe with MAS = 8 kHz, 98 K at 14.1 T on a 3.2 mm probe with MAS = 8 kHz, and 110 K at 18.8 T on a 1.3 mm probe with MAS = 40 kHz. For the three magnetic fields (9.4, 14.4 and 18.8 T), enhancements factors were calculated from the proline (aqueous-based PAs) or the TCE (non-aqueous-based PA) signals in ^{13}C one-dimensional ^{1}H-^{13}C CP-MAS spectra at a MAS frequency of 8 kHz (9.4 and 14.4 T) and 40 kHz (18.8 T). ^{1}H-^{13}C CP-MAS experiments were recorded using 100 kHz (for 3.2 mm) and 155 kHz (for 1.3 mm) nutation field strength for ^{1}H $\pi/2$

pulses and heteronuclear decoupling, and a ramped (50-100%) ^{1}H rf field to match a Hartman-Hahn CP condition when using a constant 50 kHz ^{13}C nutation field strength during the CP spin-locking contact time of 2 ms.

MQMAS

The ^{1}H-^{27}Al CP MQMAS NMR 2D spectrum of γ-alumina was recorded at 18.8 T, at 40 kHz MAS frequency, and a sample temperature of ~100 K. In the indirect dimension, 72 points[20] (36 complex points) were collected with a dwell time of 17.71 µs. 144 scans were recorded for each point with 5 s of recycle delay between each scan. The total experimental time was 14.4 h. The number of scans were kept at multiples of 12 to complete the phase cycling for triple quantum (3Q) selection at the conversion pulse. 150 kHz of SW$_f$-TPPM heteronuclear decoupling[21] was applied during the direct and indirect acquisition periods for 3 and 0.65 ms, respectively. After a 100 kHz 90° excitation pulse on 1H, a high-power CP of 1 ms was used to transfer the magnetization to ^{27}Al. A pulse with a phase-cycling selective of 3Q and length 0.8 µs was employed. This reconversion pulse selects the coherence order of ± 3 → 0. Subsequently a *z*-filter of 20 µs was applied followed by a CT-selective read-out π/2 pulse at a rf field strength of 20 kHz (12 µs). The RF amplitudes on ^{27}Al channel are that of the RF field in the coil, corresponding to spin-1/2 nutation frequency, and not of the central/satellite transitions. Both dimensions were apodized with a decaying exponential function of 50 Hz. The indirect dimension was referenced according to the convention Cz as given in Ref. [22] and [23]

Microwave power measurements

The 600 MHz / 395 GHz / 14.1 T MAS-DNP spectrometer uses a quasi-optical bench previously described.[24] This allows measuring the microwave power at the end of the tapper, before the Martin-Puplett interferometer as shown

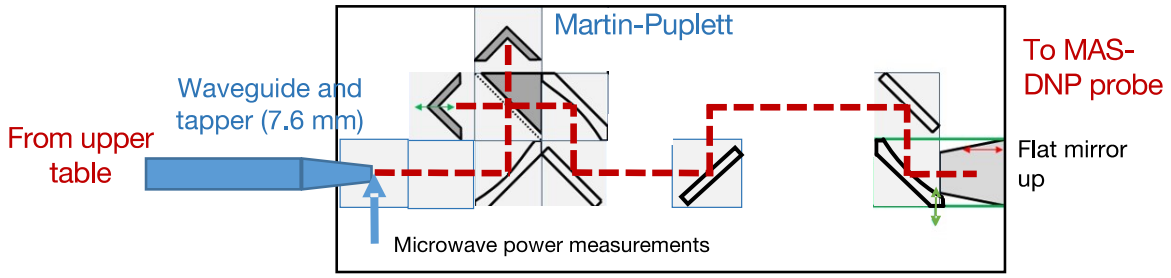

Fig S. 5 Quasi-optic bench between the gyrotron and the MAS-DNP probe. The beam power is measured at the end of the 7.6 mm tapper

Sample preparation

Frozen solutions

The following radical frozen solution were prepared: (i) PyrroTriPol and TEMTriPol-I were dissolved to reach the desired concentration (10 or 5 mM) in a deuterated DNP matrix. The deuterated DNP matrix was a mixture of d_8-glycerol/D_2O/H_2O (60:30:10; v:v:v) containing 0.25 M of U-^{13}C,^{15}N-proline; (ii) of PyrroTriPol-OMe and TEMTriPol-I-OMe were dissolved to reach a concentration of 16 mM in 1,1,2,2-tetra-chloroethane (TCE). 25 µL of solution were packed in a 3.2 mm sapphire rotor (for the 3.2 mm probe at 9.4 and 14.1 T), without silicon plug and closed with a Vespel cap. For PyrroTriPol-OMe and TEMTriPol-I-OMe, 30 µL of frozen solution was mixed with 30 mg of hexagonal boron nitride (hBN). 25 mg of this final DNP sample was then packed into a 3.2 mm sapphire rotor (for the 3.2 mm probe at 9.4 and 14.1 T) without silicon plug and closed with a Vespel cap. Prior to DNP experiments, the TCE-based samples were degassed *in-situ* by repeating 5 cycles of eject/insert inside the probe. For the 1.3 mm probes (18.8 T), $\approx$ 3 µL of each radical frozen solution (PyrroTriPol, TEMTriPol-I, PyrroTriPol-OMe and TEMTriPol-I-OMe) were packed in a 1.3 mm zirconia rotor and closed with a Vespel cap. No *h*BN particles were added into the 1.3 mm rotors.

γ-alumina sample

Samples of γ-Al_2O_3 (nanopowder < 50 nm particle size), were purchased from Sigma Aldrich and used as received without further purification. Approximately 30 mg of the alumina powder was impregnated with a solution of PyrroTriPol-OMe (30 µL, 16 mM) in TCE. Prior to impregnation, the alumina powder was heated at T = 90 °C for 12 h to remove the moisture from the alumina surface. In addition, the radical solution in TCE was degassed using N_2 gas in order to remove moisture as well. The DNP sample was then packed into a 1.3 mm zirconia rotor. The total weight of sample inside the rotor was estimated to be 2 mg by weighing the rotor before and after packing of the sample.

Microcrystalline powders

Cellulose and adenosine were purchased from Sigma Aldrich and used as received without further purification.
Prior to sample preparation, the cellulose and the adenosine powders were ground by hand using a mortar to reduce the grain size. For each compound, the following samples were prepared for DNP:

1. 30 mg of cellulose powder impregnated with 30 µL of radical solution containing 10 mM PyrroTriPol or TEMTriPol-I in the deuterated DNP matrix of d_8-glycerol/D_2O/H_2O (60:30:10; v:v:v)
2. 30 mg of adenosine powder impregnated with 20 µL of radical solution containing 16 mM PyrroTriPol-OMe or TEMTriPol-I-OMe in TCE.
3. 30 mg of adenosine powder impregnated with 20 µL of radical solution containing 11 mM DiPyrroTriPol-OMe and DiTEMTriPol-I-OMe in TCE.

The samples were than packed into a 3.2 mm sapphire rotor. The total weight of sample inside the rotor was estimated to be ~ 30 mg by weighing the rotor before and after packing of the sample.

Quenching factor measurements and concentration dependency of the DNP efficiency

The quenching factor, $\epsilon_{Bleaching/Quenching}$[25] or χ_{Bleach}[15], which represents the proportion of detectable nuclei was measured by separately quantifying the contribution factor,[26] $\theta = \epsilon_{Bleaching/Quenching} \times \epsilon_{Depo}$ and the depolarisation factor ϵ_{Depo}. The measurements were carried out at 14.1 T and 7.3 kHz. The ^{13}C CP NMR signal intensity of a 16 mM PyrroTriPol-OMe in TCE, I_{doped}, and pure TCE solution, $I_{undoped}$, were measured at steady state in absence of microwave irradiation. To ensure that the steady state was reached, recycling delay was set to $5 \times T_{1,n}$ corresponding to 10 s for the doped sample, and 2500 s for the undoped sample.
We obtained

$$\theta = \frac{I_{doped}}{I_{undoped}} = 0.75 \pm 0.05$$

In addition, we also measured a depolarization factor $\epsilon_{depo} = 0.9 \pm 0.05$. From these measurements, we can extract a bleaching/quenching factor $\epsilon_{Bleaching/Quenching} = 0.83 \pm 0.1$. This value in very good agreement with previous measurements for 12 mM AMUPol (0.85).[25]

Table S2 Concentration dependence of PyrroTriPol and PyrroTriPol-OMe at 8 kHz, and 14.1 T.

Biradical	Concentration (mM)	$\epsilon_{on/off}$,	ϵ_B	ϵ_{Depo}	T_B (s)
PyrroTriPol	3	105			6.3
	5	80 ± 2	76 ± 6	0.95 ± 0.05	4.5
	10	64-74	58-66	0.92 ± 0.05	2.1-2.8
PyrroTriPol-OMe	10	95	-	-	3.8
	16	106	98	0.92	2.4

Additional Triradicals results

Experimental performance of DiTEMTriPol-I-OMe and DiPyrroTriPol-OMe on small molecules

The experimental performance of the Tri-radicals was measured on adenosine impregnated with 11 mM solution of DiTEMTriPol-I-OMe or DiPyrroTriPol-OMe in TCE. The optimal recycling delay and the corresponding comparison of sensitivity is reported in ref. [12]. Overall DiPyrroTriPol-OMe provides a better sensitivity by almost a factor 4 despite a slightly slower T_{opt}.

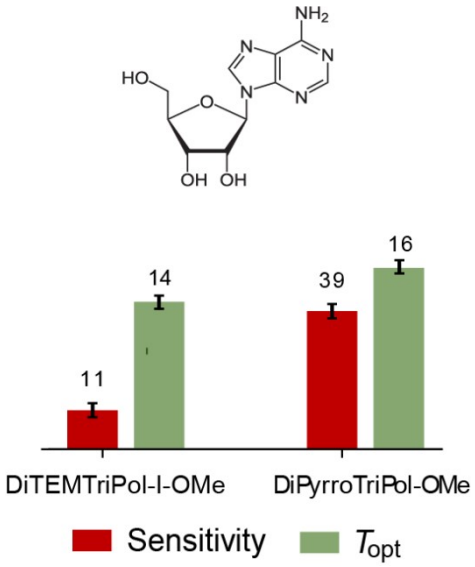

Fig S. 6 Experimental sensitivity and optimal recycling delays for 11 mM DiTEMTriPol-I-OMe and DiPyrroTriPol-OMe in TCE applied to adenosine, measured at 8 kHz MAS, 9.4 T and 100 K (3.2 mm rotors).

Simulations of the MAS-DNP field profile of PyrroTriPol-OMe and DiPyrroTriPol-OMe

We carried out additional simulations to assess PyrroTriPol-OMe vs DiPyrroTriPol-OMe. Two sets of MAS-DNP simulations were carried out using a small spin system made of one strongly connected proton, one trityl and one or two nitroxide. In all simulations we assumed that the nuclear relaxation was relatively fast, i.e. 40 ms, when the dipolar hyperfine coupling is 3 MHz. This was based on previous quantitative simulations.[11] We used such fast relaxing protons to discriminate the effect of the Cross-Effect rotor events (see ref [27] for details).

Two sets of simulations were carried out: one set where the 1H is connected to the Trityl, one set where it is connected to the Nitroxide. Experimentally, *the first set of simulations is not realistic as the Trityl does not possess strongly coupled protons*. The MAS-DNP simulations in **Fig S. 7** (a) show how the simulated DNP profile compares between three cases: a PyrroTriPol-OMe, and DiPyrroTriPol-OMe assuming the presence or absence of nitroxide-nitroxide dipolar interaction. First, one can notice that the presence of the weak nitroxide(1)-nitroxide(2) coupling does not significantly affect the MAS-DNP performance. Second, un these simulations, DiPyrroTriPol-OMe clearly outperforms PyrroTriPol-OMe. However, **Fig S. 7** (b), where the 1H is connected to the Nitroxide, PyrroTriPol-OMe is equivalent to DiPyrroTriPol-OMe and there are no benefits from a Triradical in that case.

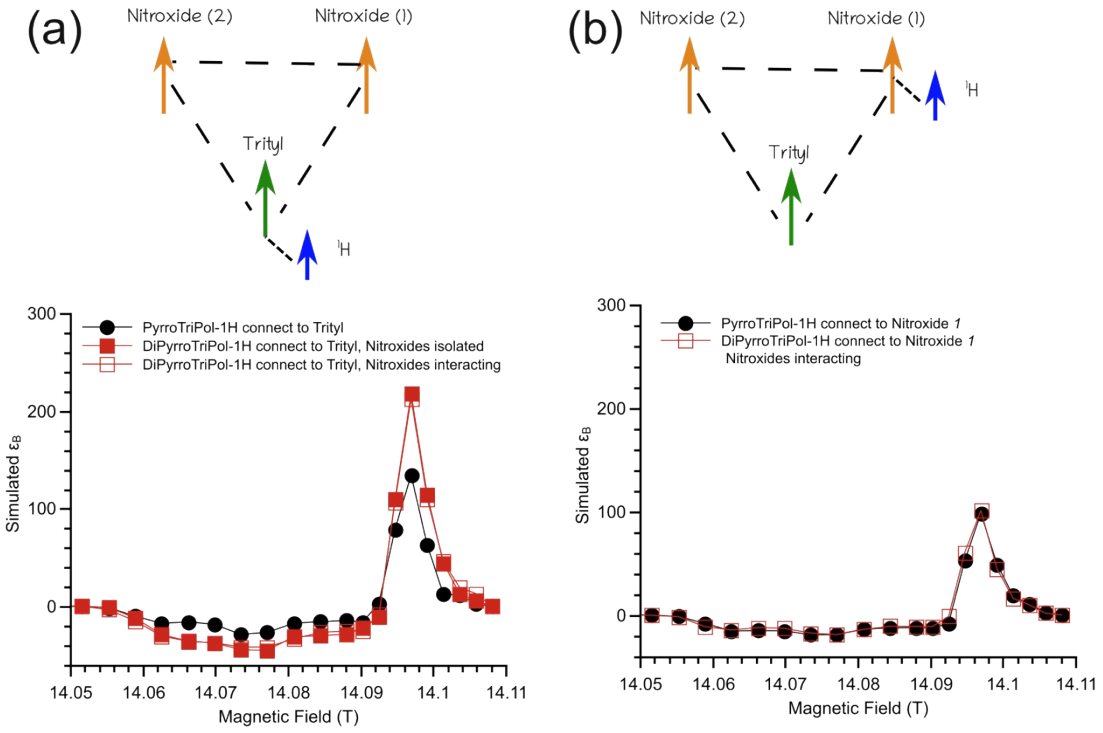

Fig S. 7 (a) top, schematical representation of the simulated spin system, bottom simulated MAS-DNP profiles of PyrroTriPol-OMe (black circles) and DiPyrroTriPol-OMe (red squares). (b) top, schematical representation of the simulated spin system, bottom MAS-DNP performance of DiPyrroTriPol-OMe (red empty squares) and DiPyrroTriPol-OMe neglecting the nitroxide-nitroxide coupling (red full squares).

The improved performance of DiPyrroTriPol-OMe in **Fig S. 7** (a) can be explained as follows: as the 1H is connected to the Trityl, it undergoes, on average, twice as many Cross-Effect rotor events per rotor cycle as compared to PyrroTriPol-OMe. The larger number of CE rotor event in DiPyrroTriPol-OMe enables the fast relaxing 1H, to be better hyperpolarized as compared to PyrroTriPol. However, in **Fig S. 7** (b), the 1H undergoes the same number of CE rotor event per rotor cycle in both PyrroTriPol-OMe and DiPyrroTriPol-OMe, thus the two polarizing agents are equivalent.
All in all, "more realistic" simulations with a fast-relaxing proton are required to really assess the potential benefits of triradicals. This is beyond the scope of this article.

The simulations were carried out using the latest version of an home-written MAS-DNP simulation tool[28]. The parameters used are reported below

- Electron relaxation times; $T_{1,e}^{Trityl} = 1$ ms; $T_{1,e}^{Tempo} = 0.2$ ms ; $T_{2,e}^{Trityl} = 2$ µs; $T_{2,e}^{Tempo} = 2$ µs;
- Nuclear relaxation times $T_{1,n} = 40$,s; $T_{2,n} = 20$ ms
- PyrroTriPol-OMe extended Trityl g-tensor: [2.0024,2.0029,2.0036]; Nitroxide [2.0081,2.0059,2.0021] and their relative orientation in degrees [163, 92, 26];
- DiPyrroTriPol-OMe extended Trityl g-tensor: [2.0024,2.0029,2.0036]; Nitroxide [2.0081,2.0059,2.0021] and their relative orientation in degrees [103, 47, 47] between Trityl and nitroxide 1; [155, 156, 58] between Trityl and nitroxide 2;
- Dipolar/Exchange interaction 21 / -8 MHz and dipolar vector between Trityl and nitroxide, $[\phi,\theta] = [-16, 101]$ degrees for PyrroTriPol-OMe
- Dipolar/Exchange interaction 21 / -8 MHz and dipolar vector between Trityl and nitroxide 2, $[\phi,\theta] =$ [-44, 111] degrees for DiPyrroTriPol-OMe
- Dipolar/Exchange interaction 8 / 0 MHz and dipolar vector between nitroxide 1 and nitroxide 2, $[\phi,\theta] =$ [-132, 71] degrees for DiPyrroTriPol-OMe
- Hyperfine coupling between Trityl and 1H or Nitroxide (1) and 1H: dipolar coupling of 3 MHz, with dipolar vector $[\phi,\theta] =$ [-0, 0] degrees
- MAS frequency: 8 kHz,
- Temperature: 100 K
- µw frequency: 395.145 GHz
- µw nutation frequency: 0.2 MHz.

- Adaptive integration convergence criteria [1e-6, 1e-3] around rotor events and away from rotor event respectively, as defined in reference [28]
- Maximum number of angular steps 2^{13}

Note that the magnetic parameters for the bi and triradicals were extracted from DFT simulations.

Simulations of the MAS-DNP power dependence for PyrroTriPol-OMe and TEKPol

Figure S8 (a) shows the experimental and simulated enhancements of PyrroTriPol-OMe and TEKPol at 14.1 T. The correspondence between power and μw nutation was obtained from previous work where it was determined that 12 W is equivalent to 0.4 MHz.[11] The parameters used for TEKPol were extracted from a previous publication.[29] Using the scaling factor between power and nutation, we calculated the power dependence of the enhancement and obtained a good agreement between experiments and simulations at 14.1 T for both biradicals in the low power domain. For PyrroTriPol-OMe, we observe that beyond 8 W, simulations and experiments start to differ. For TEKPol, the simulation curve overestimate the enhancement beyond 7 W. To explain this discrepancy, we hypothesize that larger μw power lead to sample heating which negatively impacts the DNP in the experiments. We thus considered that below 6 W the sample heating was not significant and thus, curves were normalized with respect to the enhancements obtain at 6 W.
From there we extrapolated the computations to the 9.4 T case for PyrroTriPol **Fig S. 8** (b). The simulation predicts that 500 mW would be sufficient to reach 50% of the maximum enhancement in a 3.2 mm rotor.

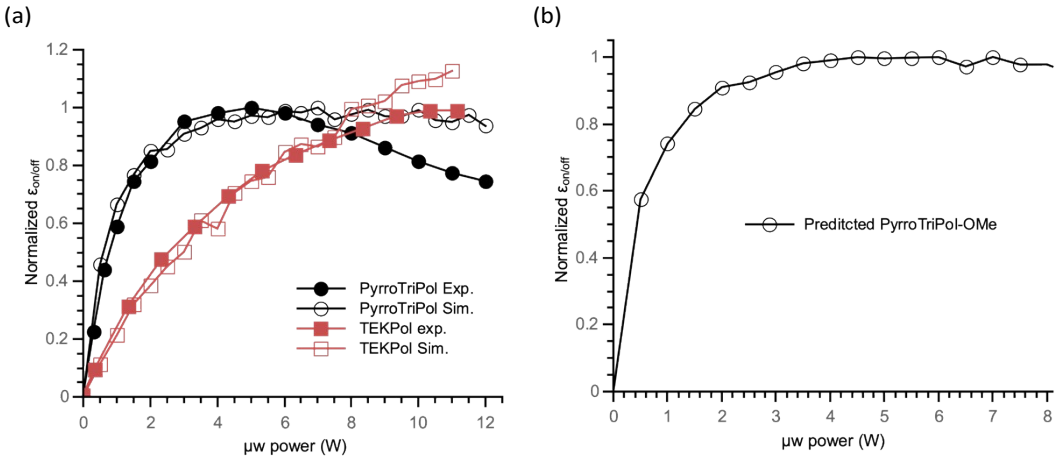

Fig S. 8 ((a) Normalized experiment (full symbols) and simulations (empty symbols) of the enhancement under MAS-DNP as a function for μw power at 14.1 T PyrroTriPol-OMe (black circles) and TEKPol (red squares). (b) Simulated MAS-DNP performance at 9.4 T as a function for μw power for PyrroTriPol-OMe (black open circles).

Simulations of the MAS dependence of PyrroTriPol-OMe

Fig. S. 9 shows the simulated (a) depolarization factor ϵ_{Depo}, (b) polarisation gain ϵ_B, for PyrroTriPol-OMe at 18.8 T for both conformer #1 and conformer #2, as well as the corresponding weighted average structure. Since conformer #1 and conformer #2 are present in a 80:20 ratio, $\epsilon_{Depo}^{avg} = 0.8\epsilon_{Depo}^{\#1} + 0.2\epsilon_{Depo}^{\#2}$ and $\epsilon_B = 0.8\epsilon_B^{\#1} + 0.2\epsilon_B^{\#2}$.Using the approach, we can also compute an average DNP enhancement factor, $\epsilon_{on/off}^{avg} = \epsilon_B^{avg}/\epsilon_{Depo}^{avg} \sim 150$ which is close to the value measured experimentally. The simulations below show that ϵ_{Depo}^{avg} decreases by ~3-4% from 10 to 40 kHz, and that ϵ_B^{avg} is nearly flat.

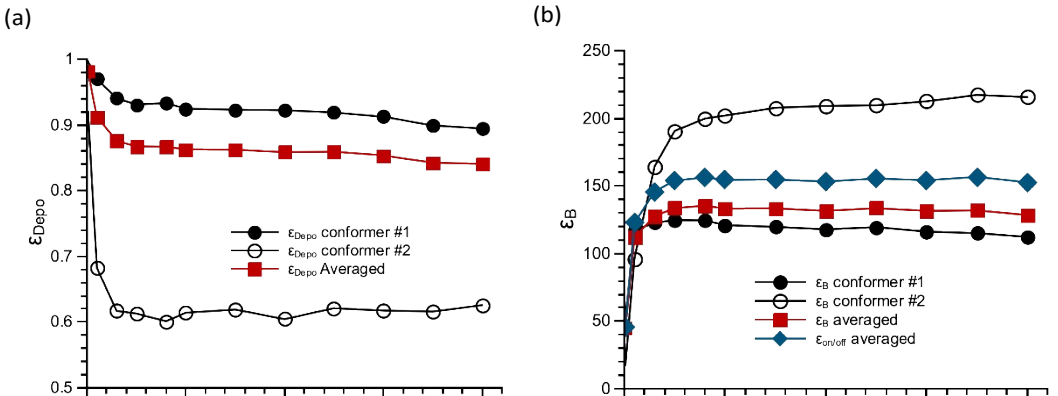

Fig S. 9 MAS-DNP simulations of the depolarization ϵ_{Depo} (a), and the polarization gain ϵ_B (b) as a function of MAS spinning frequency at 18.8 T. Black full circles corresponds to PyrroTriPol-OMe conformer #1, black open circles, to conformers #2, red squares to the average depolarization (or polarization gain) obtained using 80% of conformer #1 and 20% of conformer #2. The blue diamonds correspond to the average $\epsilon_{on/off} = \epsilon_B / \epsilon_{Depo}$

References

1 A. A. Bobko, I. Dhimitruka, J. L. Zweier and V. V. Khramtsov, Trityl radicals as persistent dual function pH and oxygen probes for in vivo electron paramagnetic resonance spectroscopy and imaging: Concept and experiment, *Journal of the American Chemical Society*, 2007, **129**, 7240–7241.

2 T. J. Reddy, T. Iwama, H. J. Halpern and V. H. Rawal, General Synthesis of Persistent Trityl Radicals for EPR Imaging of Biological Systems, *The Journal of Organic Chemistry*, 2002, **67**, 4635–4639.

3 F. Neese, The ORCA program system, *Wiley Interdisciplinary Reviews: Computational Molecular Science*, 2012, **2**, 73–78.

4 S. Grimme, J. G. Brandenburg, C. Bannwarth and A. Hansen, Consistent structures and interactions by density functional theory with small atomic orbital basis sets, *The Journal of Chemical Physics*, 2015, **143**, 054107.

5 T. Yanai, D. P. Tew and N. C. Handy, A new hybrid exchange–correlation functional using the Coulomb-attenuating method (CAM-B3LYP), *Chemical Physics Letters*, 2004, **393**, 51–57.

6 T. Lu and F. Chen, Multiwfn: A multifunctional wavefunction analyzer, *Journal of Computational Chemistry*, 2012, **33**, 580–592.

7 P. Eastman, J. Swails, J. D. Chodera, R. T. McGibbon, Y. Zhao, K. A. Beauchamp, L.-P. Wang, A. C. Simmonett, M. P. Harrigan, C. D. Stern, R. P. Wiewiora, B. R. Brooks and V. S. Pande, OpenMM 7: Rapid development of high performance algorithms for molecular dynamics, *PLOS Computational Biology*, 2017, **13**, e1005659.

8 S. Grimme, A. Hansen, S. Ehlert and J.-M. Mewes, r 2 SCAN-3c: A “Swiss army knife” composite electronic-structure method, *The Journal of Chemical Physics*, 2021, **154**, 064103.

9 C. Adamo and V. Barone, Toward reliable density functional methods without adjustable parameters: The PBE0 model, *The Journal of Chemical Physics*, 1999, **110**, 6158–6170.

10 F. Weigend, Accurate Coulomb-fitting basis sets for H to Rn, *Physical Chemistry Chemical Physics*, 2006, **8**, 1057.

11 F. Mentink-Vigier, T. Dubroca, J. van Tol and S. T. Sigurdsson, The distance between g-tensors of nitroxide biradicals governs MAS-DNP performance: The case of the bTurea family, *Journal of Magnetic Resonance*, 2021, **329**, 107026.

12 R. Harrabi, T. Halbritter, F. Aussenac, O. Dakhlaoui, J. van Tol, K. K. Damodaran, D. Lee, S. Paul, S. Hediger, F. Mentink-Vigier, S. Th. Sigurdsson and G. De Paëpe, Highly Efficient Polarizing Agents for MAS-DNP of Proton-Dense Molecular Solids, *Angewandte Chemie International Edition*, , DOI:10.1002/anie.202114103.

13 J. van Tol, L.-C. Brunel and R. J. Wylde, A quasioptical transient electron spin resonance spectrometer operating at 120 and 240 GHz, *Review of Scientific Instruments*, 2005, **76**, 074101.

14 G. Mathies, M. A. Caporini, V. K. Michaelis, Y. Liu, K. N. Hu, D. Mance, J. L. Zweier, M. Rosay, M. Baldus and R. G. Griffin, Efficient Dynamic Nuclear Polarization at 800 MHz/527 GHz with Trityl-Nitroxide Biradicals, *Angewandte Chemie - International Edition*, 2015, **54**, 11770–11774.

15 F. Mentink-Vigier, G. Mathies, Y. Liu, A.-L. Barra, M. A. Caporini, D. Lee, S. Hediger, R. G. Griffin and G. De Paepe, Efficient cross-effect dynamic nuclear polarization without depolarization in high-resolution MAS NMR, *Chemical Science*, 2017, **8**, 8150–8163.

16 S. Stoll and R. D. Britt, General and efficient simulation of pulse EPR spectra., *Phys Chem Chem Phys*, 2009, **11**, 6614–25.

17 Q. Chen, S. S. Hou and K. Schmidt-Rohr, A simple scheme for probehead background suppression in one-pulse 1H NMR, *Solid State Nuclear Magnetic Resonance*, 2004, **26**, 11–15.

18 D. Wisser, G. Karthikeyan, A. Lund, G. Casano, H. Karoui, M. Yulikov, G. Menzildjian, A. C. Pinon, A. Purea, F. Engelke, S. R. Chaudhari, D. Kubicki, A. J. Rossini, I. B. Moroz, D. Gajan, C. Copéret, G. Jeschke, M. Lelli, L. Emsley, A. Lesage and O. Ouari, BDPA-Nitroxide Biradicals Tailored for Efficient Dynamic Nuclear Polarization Enhanced Solid-State NMR at Magnetic Fields up to 21.1 T, *J. Am. Chem. Soc.*, 2018, **140**, 13340–13349.

19 K. R. Thurber and R. Tycko, Measurement of sample temperatures under magic-angle spinning from the chemical shift and spin-lattice relaxation rate of 79Br in KBr powder, *Journal of Magnetic Resonance*, 2009, **196**, 84–87.

20 D. Marion and K. Wüthrich, Application of phase sensitive two-dimensional correlated spectroscopy (COSY) for measurements of 1H-1H spin-spin coupling constants in proteins, *Biochemical and Biophysical Research Communications*, 1983, **113**, 967–974.

21 R. S. Thakur, N. D. Kurur and P. K. Madhu, Swept-frequency two-pulse phase modulation for heteronuclear dipolar decoupling in solid-state NMR, *Chemical Physics Letters*, 2006, **426**, 459–463.

22 M. Hanaya and R. K. Harris, Optimization of Two-Dimensional Multiple-Quantum MAS NMR Experiments for I = 3 / 2 Nuclei on a Moderate-Field Spectrometer, *The Journal of Physical Chemistry A*, 1997, **101**, 6903–6910.

23 P. P. Man, Scaling and labeling the high-resolution isotropic axis of two-dimensional multiple-quantum magic-angle-spinning spectra of half-integer quadrupole spins, *Physical Review B*, 1998, **58**, 2764–2782.

24 T. Dubroca, A. N. A. N. Smith, K. J. K. J. Pike, S. Froud, R. Wylde, B. Trociewitz, J. E. McKay, F. Mentink-Vigier, J. van Tol, S. Wi, W. W. Brey, J. R. Long, L. Frydman and S. Hill, A quasi-optical and corrugated waveguide microwave transmission system for simultaneous dynamic nuclear polarization NMR on two separate 14.1 T spectrometers, *J. Magn. Reson.*, 2018, **289**, 35–44.

25 F. Mentink-Vigier, S. Paul, D. Lee, A. Feintuch, S. Hediger, S. Vega and G. De Paëpe, Nuclear depolarization and absolute sensitivity in magic-angle spinning cross effect dynamic nuclear polarization, *Phys. Chem. Chem. Phys.*, 2015, **17**, 21824–21836.

26 S. R. Chaudhari, P. Berruyer, D. Gajan, C. Reiter, F. Engelke, D. L. Silverio, C. Copéret, M. Lelli, A. Lesage and L. Emsley, Dynamic nuclear polarization at 40 kHz magic angle spinning, *Phys. Chem. Chem. Phys.*, 2016, **18**, 10616–10622.
27 F. Mentink-Vigier, U. Akbey, H. Oschkinat, S. Vega and A. Feintuch, Theoretical aspects of Magic Angle Spinning - Dynamic Nuclear Polarization, *J. Magn. Reson.*, 2015, **258**, 102–120.
28 F. Mentink-Vigier, Numerical recipes for faster MAS-DNP simulations, *Journal of Magnetic Resonance*, 2021, **333**, 107106.
29 F. Mentink-Vigier, A.-L. Barra, J. van Tol, S. Hediger, D. Lee and G. De Paepe, De novo prediction of cross-effect efficiency for magic angle spinning dynamic nuclear polarization, *Physical Chemistry Chemical Physics*, 2019, **21**, 2166–2176.